Macroscopic quantum coherence and mechanical squeezing of a graphene sheet

Xiyun Li,[1] Wenjie Nie,[1,*] Aixi Chen,[2,†] and Yueheng Lan[3,‡]

[1]*Department of Applied Physics, East China Jiaotong University, Nanchang 330013, China*
[2]*Department of Physics, Zhejiang Sci-Tech University, Hangzhou 310018, China*
[3]*Department of Physics, Beijing University of Posts and Telecommunications, Beijing 100876, China*

We theoretically investigate the macroscopic quantum coherence and the mechanical squeezing of a mechanical oscillator in a hybrid optomechanical system consisting of a suspended graphene sheet and an ultracold atomic ensemble trapped inside a Fabry-Pérot cavity. In the study the vacuum is used to mediate an effective optomechanical coupling between the graphene oscillator and the cavity field driven by an external laser beam. We find that in the presence of this coupling, the macroscopic quantum coherence and the mechanical squeezing of the graphene sheet can be attained in a certain range of driving power. In particular, the quantum coherence in the optomechanical system can be transferred from the optical field to the mechanical oscillator. We also investigate in detail the spectrum and the squeezing of the output field and the attained results may be used to study the mechanical squeezing of a graphene sheet.

I. INTRODUCTION

It is well known that the internal degrees of freedom of an atom can be coupled to a light field with a small atom-field detuning, which implies that the propagation of a weak light field in atom-field-coupled systems can be coherently manipulated through another strong-coupling field. In general, the atom in these systems is described by a three-level system so that the quantum interference between different pathways of excitation in the system induces a fascinating phenomenon called the electromagnetically induced transparency [1–4], which is important for the light control and storage as well as the production of giant nonlinear effects [5,6]. Moreover, the atom-light interaction inside an optical cavity has been extended to the study of the linear optomechanical coupling between a light field and a collection of atoms, i.e., the Bose-Einstein condensate [7,8]. The coherent coupling of the mechanical element with the light field in the optomechanical system can be also used for modulating the propagation of the light field [9,10], which is demonstrated by the adjustable width of the transparency window.

In optomechanics, the main aim is to manipulate and enhance the effective coupling between a light field and a massive mechanical oscillator via radiation pressure. The radiation pressure of the light field also influences the interesting dynamics of macroscopic mechanical motions. In this regard, various coupled systems, i.e., a Fabry-Pérot cavity with a movable end mirror [11,12], a levitated nanosphere optomechanical system [13–17], and an embedded membrane optical cavity [18,19], have been proposed to promote the effective optomechanical coupling. In these optomechanical systems, the optical cavity is driven strongly by an external laser beam which shines directly on the movable elements so as to induce a considerable radiation pressure on these mechanical oscillators. The optomechanical coupling has also been realized in other types of optomechanical systems, such as a microresonator in a whispering-gallery cavity [20,21] and a microwave transmission line resonator [22–24]. From the application point of view, a strong optomechanical coupling helps one explore the quantum-mechanical effect of the macroscopic resonator, i.e., by optomechanical entanglement [11,17,25–28], the optical cooling of the mechanical mode [29,30], and the mechanical state preparation [31,32]. In addition, a mechanical and an optomechanical coherence in a macroscopic system are investigated in detail, which is waiting to be probed [33]. The quantum coherence of a mechanical oscillator requires less than one thermophonon on each mechanical cycle to persist, which may be doable in current experiments [34–38]. The squeezed mechanical state is also an important characteristic of the optomechanical system [39–43], which can be used to improve the precision of quantum measurements at the expense of other components of the quadrature uncertainty [44]. In particular, the detection accuracy of the signal in the quantum resonator is only limited by the ability to prepare the chosen quadrature in a low uncertainty state, which is often used for quantum measurements [45] and quantum information [46].

As opposed to the direct optomechanical interaction between a cavity field and a mechanical oscillator, an optomechanical coupling between a light field and a massive oscillator can be generated by the internal state of an atomic ensemble [47] or an electron spin accumulated in a carbon nanotube [48], in which various quantum-mechanical properties of mechanical motions can be discussed in detail. In this work, by combining the mechanical system and cavity quantum electrodynamics [49], we propose an optomechanical scheme to realize an effective optomechanical coupling between a graphene sheet and a cavity field, which is mediated by the vacuum-induced interaction between the graphene sheet and the internal states of an ultracold atomic ensemble. Further, we focus on the study of the macroscopic quantum coherence and the mechanical squeezing of the graphene sheet in the hybrid optomechanical system and discuss in detail their dependence on the distance between the atoms and the graphene sheet and on the atom-field coupling strength. We show that the

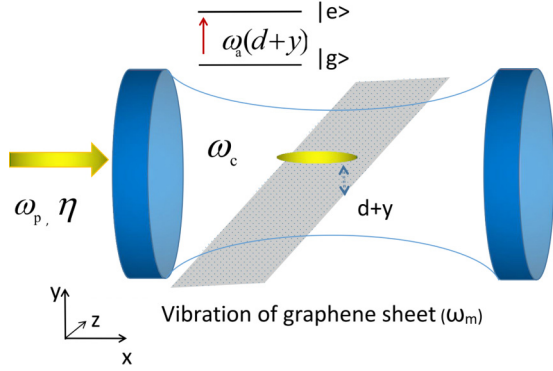*niewenjiezhu@sina.cn
†aixichen@163.com
‡lanyh@bupt.edu.cn

FIG. 1. Plot of the setup studied in the paper. An ensemble of N two-level ultracold atoms is trapped inside an optical cavity, which interacts with a driven cavity mode ω_c and a suspended graphene sheet. Vibration of the graphene sheet changes the internal state of the atoms due to the vacuum fluctuation. The cavity mode is driven by a classical laser with frequency ω_p and amplitude η.

quantum coherence and the mechanical squeezing of the graphene sheet can be greatly enhanced via the vacuum effect and the atom-field coupling. In particular, the behavior of quantum coherence in the optomechanical system can be transferred from the optical field to the mechanical oscillator. We also investigate in detail the occurrence of the normal-mode splitting in the spectrum of the output field and its squeezing.

The paper is organized as follows. In Sec. II, we give the model and the Hamiltonian of system. In Sec. III, we derive the quantum Langevin equation and linearize it to obtain the dynamics of quantum fluctuations around the steady-state expectation values. Further, we calculate the quadrature fluctuations of the graphene sheet and the cavity field. In Secs. IV and V, we discuss how the macroscopic quantum coherence and mechanical squeezing of a graphene sheet can be realized by changing the system parameters. In Sec. VI, we discuss the spectrum of the output field and its squeezing. Our conclusions are given in Sec. VII.

II. MODEL

As depicted in Fig. 1, we consider an ensemble of N two-level ultracold ^{87}Rb atoms in a high-Q optical cavity with generic frequency ω_c, which is driven through one of the end mirrors by a classical laser with frequency ω_p and amplitude η. The bare transition frequency between the ground state $|g\rangle = |F = 1\rangle$ and the excited state $|e\rangle = |F' = 2\rangle$ of the D_2 line of ^{87}Rb is denoted as ω_0. We assume that the atomic ensemble is confined in a cylindrically symmetric trap with a transverse trapping frequency $\omega_\perp$ and negligible longitudinal confinement along the x direction [50]. The additional mechanical oscillator in the system is a suspended graphene sheet placed in the x-z plane, which approaches the ultracold atoms and changes the transition frequencies of atoms by the vacuum fluctuation effect [51,52]. That is, the transition frequency ω_a of a two-level atom is modulated by the distance between the atom and the graphene, i.e., $\omega_a(d + y) = \omega_0 + \Delta\omega_a(d + y)$, where $\Delta\omega_a(d + y)$ is the frequency shift of the atom due to the vacuum fluctuation [52], d is the distance between the atom and the graphene in the static atom-plane

geometry, and y is the position of the graphene sheet. In addition, it is noted that the graphene sheet placed in the x-z plane is similar to a transverse micromechanical cantilever such that the light radiation pressure on the graphene sheet is negligible because light shining on the sheet is reflected back inefficiently [53].

Further, we consider the dispersive regime with a large atom-pump detuning and low saturation, i.e., $\omega_p \gg \omega_a(d + y)$ and $\Delta_a(d + y) = \omega_p - \omega_a(d + y) \gg \Gamma_0$, so that the excited atomic state can be eliminated adiabatically [54,55]. Here Γ_0 is the decay rate of the atom. In the frame rotating at the pump frequency, the many-body Hamiltonian reads

$$H = -\hbar\Delta_c a^\dagger a - i\hbar\eta(a - a^\dagger) + \int_{-\frac{L}{2}}^{\frac{L}{2}} \Psi^\dagger(x)\left[\frac{p_x^2}{2m_a}\right.$$
$$\left. + \hbar U_0(d + y)\cos^2(kx)a^\dagger a\right]\Psi(x)dx + \frac{p_y^2}{2M} + \frac{M}{2}\omega_m^2 y^2, \tag{1}$$

where $\Delta_c = \omega_p - \omega_c$ is the cavity-pump detuning; k is the wave number of the cavity field; a ($a^\dagger$) is the annihilation (creation) operator of the optical field; and the amplitude of the external driving laser $|\eta| = \sqrt{\frac{2P\kappa}{\hbar\omega_p}}$, where κ is the decay rate of the optical field and P is the laser power. M and ω_m are the effective mass and the oscillation frequency of the graphene sheet, respectively. The position and momentum of the graphene sheet, y and p_y, satisfy the commutation relation $[y, p_y] = i\hbar$. $U_0(d + y) = \frac{g_0^2}{\Delta_a(d + y)}$ is the optical lattice barrier height per photon, which includes the mechanical and atomic back-actions on the field. g_0 is the vacuum Rabi frequency and m_a is the mass of the single ^{87}Rb atom. We use a first-order approximation of the frequency shift $\Delta\omega_a(d + y)$, i.e., $\Delta\omega_a(d + y) = \Delta\omega_a(d) + \lambda_0(d)y$, so that the atom-pump detuning becomes $\Delta_a(d + y) \simeq \Delta_a(d) - \lambda_0(d)y$. Here $\lambda_0(d) = \frac{\partial\Delta\omega_a(d + y)}{\partial y}|_{y=0}$ is the vacuum-induced coupling between the atom and the graphene sheet [51,52], which depends strongly on the atom-graphene distance d and can be calculated in terms of the level shift of the atom between its ground and excited states (see the Appendix).

$\Psi(x)$ is the bosonic annihilation operator for the atomic field, which can be expanded as the following single-mode quantum field in the weak field and Bogoliubov approximation [8,56,57]:

$$\Psi(x) = \sqrt{\frac{N}{L}} + \sqrt{\frac{2}{L}}\cos(2kx)c, \tag{2}$$

where the operator c is the bosonic annihilation operator for the Bogoliubov mode. Substituting this expansion into Eq. (1) and taking the position and momentum operators nondimensionalized as $\sqrt{\frac{M\omega_m}{\hbar}}y \to y$ and $\sqrt{\frac{1}{\hbar M\omega_m}}p_y \to p_y$, respectively, the Hamiltonian of the system is written as

$$H = -\hbar\left[\Delta_c - \frac{N}{2}U_1(d + y)\right]a^\dagger a + \hbar\Omega_c c^\dagger c + \frac{\hbar\omega_m}{2}\left(p_y^2 + y^2\right)$$
$$- i\hbar\eta(a - a^\dagger) + \hbar\frac{\sqrt{2N}}{4}U_1(d + y)a^\dagger a(c + c^\dagger), \tag{3}$$

where $\Omega_c = \frac{2\hbar k^2}{m_a}$ denotes the frequency of the Bogoliubov mode. In deriving Eq. (3), we redefined the dimensionless coupling strength, i.e., $\lambda_1 = \lambda_0 \sqrt{\frac{\hbar}{M\omega_m}}$, and the corresponding optical lattice potential, i.e., $U_1(d+y) = \frac{g_0^2}{\Delta_a(d) - \lambda_1 y}$. It is found from Eq. (3) that the optical lattice potential induces the coupling between the atomic ensemble and the graphene as well as the optomechanical coupling between the cavity field and the graphene sheet. Furthermore, both the atom-graphene and the field-graphene couplings result from the atomic vacuum effect.

III. QUANTUM DYNAMICS AND FLUCTUATIONS

A complete dynamical analysis of an open system should include fluctuation-dissipation processes affecting the optical field, the oscillating graphene sheet, and the atomic ensemble. Using the Hamiltonian Eq. (3) and taking into account the noise effects, the Heisenberg-Langevin equations of motion describing the quantum dynamics of the hybrid system are derived as

$$\dot{y} = \omega_m p_y,$$

$$\dot{p}_y = -\omega_m y - \frac{\lambda_1 U_1(d+y)}{\Delta_a(d) - \lambda_1 y}\left[\frac{N}{2} + \frac{\sqrt{2N}}{4}(c + c^\dagger)\right]a^\dagger a$$
$$\quad - \gamma_m p_y + \xi(t),$$

$$\dot{c} = -i\Omega_c c - \gamma_a c - i\frac{\sqrt{2N}}{4}U_1(d+y)a^\dagger a + \sqrt{2\gamma_a}c_{in}(t),$$

$$\dot{a} = i\Delta_c a - \kappa a - iU_1(d+y)\left[\frac{N}{2} + \frac{\sqrt{2N}}{4}(c + c^\dagger)\right]a$$
$$\quad + \eta + \sqrt{2\kappa}a_{in}(t), \tag{4}$$

where γ_m and γ_a characterize the dissipation of the graphene sheet and the collective density excitation of the ultracold atoms, respectively. $\xi(t)$ is the Brownian noise with zero mean and the correlation [58] $\langle\xi(t)\xi(t')\rangle = \frac{\gamma_m}{\omega_m}\int\frac{d\omega}{2\pi}e^{-i\omega(t-t')}\omega[\coth(\frac{\hbar\omega}{2k_B T}) + 1]$, where k_B is the Boltzmann constant and T is the environmental temperature. The environmental input noise for the cavity field, $a_{in}(t)$, and the thermal input noise for the Bogoliubov mode of the atomic ensemble, $c_{in}(t)$, have the same correlation relation, i.e., $\langle a_{in}(t)a_{in}^\dagger(t')\rangle = \delta(t - t')$, $\langle c_{in}(t)c_{in}^\dagger(t')\rangle = \delta(t - t')$ [59].

Next we investigate the linearized dynamics of the quantum fluctuations around the steady-state expectation values of the system by decomposing each operator in Eq. (4) as the sum of its steady-state value and a small fluctuation, i.e., $O = O_s + \delta O (O = a, c, y, p_y)$. By inserting this ansatz into Eq. (4) and neglecting all the higher-order terms ($\delta O\delta O$), we can obtain the steady-state values of the system and the corresponding set of linear ordinary differential equations for the fluctuations. For example, the steady-state expectation values of the hybrid

optomechanical system are as follows:

$$p_{ys} = 0,$$

$$y_s = -\frac{\lambda_1 U_{1s}}{\omega_m \Delta_{as}}\left[\frac{N}{2} + \frac{\sqrt{2N}}{4}(c_s + c_s^\dagger)\right]|a_s|^2,$$

$$c_s = -i\frac{\sqrt{2N}}{4}\frac{U_{1s}|a_s|^2}{\gamma_a + i\Omega_c},$$

$$a_s = \frac{\eta}{\kappa - i\Delta_{\text{eff}}}, \tag{5}$$

where $U_{1s} = \frac{g_0^2}{\Delta_{as}}$ with $\Delta_{as} = \Delta_a(d) - \lambda_1 y_s$, and $\Delta_{\text{eff}} = \Delta_c - \frac{N}{2}U_{1s} - \frac{\sqrt{2N}}{4}U_{1s}(c_s + c_s^\dagger)$ is the effective detuning of cavity field. Here we assume that a_s is a real number.

Further, we introduce the Bogoliubov mode quadratures $\delta X_c = (\delta c + \delta c^\dagger)/\sqrt{2}, \delta Y_c = (\delta c - \delta c^\dagger)/\sqrt{2}i$, the cavity field quadratures $\delta X_a = (\delta a + \delta a^\dagger)/\sqrt{2}$, $\delta Y_a = (\delta a - \delta a^\dagger)/\sqrt{2}i$, and the corresponding noises $\delta X_c^{in} = (\delta c_{in} + \delta c_{in}^\dagger)/\sqrt{2}$, $\delta Y_c^{in} = (\delta c_{in} - \delta c_{in}^\dagger)/\sqrt{2}i$, $\delta X_a^{in} = (\delta a_{in} + \delta a_{in}^\dagger)/\sqrt{2}$, and $\delta Y_a^{in} = (\delta a_{in} - \delta a_{in}^\dagger)/\sqrt{2}i$. The quantum dynamics for these fluctuations can be written as

$$\delta\dot{y} = \omega_m \delta p_y,$$

$$\delta\dot{p}_y = -\omega_{m0}\delta y - \gamma_m\delta p_y - \sqrt{2}G_{yc}\delta X_c$$
$$\quad - \sqrt{2}G_{ya}\delta X_a + \xi(t),$$

$$\delta\dot{X}_c = -\gamma_a\delta X_c + \Omega_c\delta Y_c + \sqrt{2\gamma_a}\delta X_c^{in},$$

$$\delta\dot{Y}_c = -\gamma_a\delta Y_c - \Omega_c\delta X_c - 2G_{ac}\delta X_a$$
$$\quad - \sqrt{2}G_{yc}\delta y + \sqrt{2\gamma_a}\delta Y_c^{in},$$

$$\delta\dot{X}_a = -\kappa\delta X_a - \Delta_{\text{eff}}\delta Y_a + \sqrt{2\kappa}\delta X_a^{in},$$

$$\delta\dot{Y}_a = -\kappa\delta Y_a + \Delta_{\text{eff}}\delta X_a - \sqrt{2}G_{ya}\delta y$$
$$\quad - 2G_{ac}\delta X_c + \sqrt{2\kappa}\delta Y_a^{in}, \tag{6}$$

where $\omega_{m0} = \omega_m + [N + \frac{\sqrt{2N}}{2}(c_s + c_s^\dagger)]\frac{\lambda_1^2 U_{1s}}{(\Delta_{as})^2}|a_s|^2$ is the effective frequency of the oscillating graphene sheet. $G_{yc} = \frac{\sqrt{2N}}{4}\lambda_1\frac{U_{1s}}{\Delta_{as}}|a_s|^2$ is the effective coupling between the atomic ensemble and the graphene sheet, $G_{ya} = [\frac{N}{2} + \frac{\sqrt{2N}}{4}(c_s + c_s^\dagger)]\lambda_1\frac{U_{1s}}{\Delta_{as}}|a_s|$ is the effective optomechanical coupling between the cavity field and the graphene sheet, and $G_{ac} = \frac{\sqrt{2N}}{4}U_{1s}|a_s|$ is the effective coupling between the cavity field and the atomic ensemble.

In order to make the analysis easier, Eq. (6) can be written in a more compact form:

$$\dot{f}(t) = Jf(t) + n(t), \tag{7}$$

where the column vector of the fluctuation operator $f^T(t) = (\delta y(t), \delta p_y(t), \delta X_c(t), \delta Y_c(t), \delta X_a(t), \delta Y_a(t))$ and the corresponding column vector of noise $n^T(t) = (0, \xi(t), \sqrt{2\gamma_a}\delta X_c^{in}, \sqrt{2\gamma_a}\delta Y_c^{in}, \sqrt{2\kappa}\delta X_a^{in}, \sqrt{2\kappa}\delta Y_a^{in})$. J is the

drift matrix, which is given by

$$J = \begin{pmatrix} 0 & \omega_m & 0 & 0 & 0 & 0 \\ -\omega_{m0} & -\gamma_m & -\chi_1 & 0 & -\chi_2 & 0 \\ 0 & 0 & -\gamma_a & \Omega_c & 0 & 0 \\ -\chi_1 & 0 & -\Omega_c & -\gamma_a & \chi_3 & 0 \\ 0 & 0 & 0 & 0 & -\kappa & -\Delta_{\text{eff}} \\ -\chi_2 & 0 & \chi_3 & 0 & \Delta_{\text{eff}} & -\kappa \end{pmatrix},$$

where $\chi_1 = \sqrt{2}G_{yc}$, $\chi_2 = \sqrt{2}G_{ya}$, and $\chi_3 = -2G_{ac}$. When all the eigenvalues of the drift matrix have negative real parts, the solutions to Eq. (7) are stable and the stability conditions of the hybrid optomechanical system can be obtained by using the Routh-Hurwitz criteria [60].

The time-domain dynamical equation of motion [Eq. (7)] can be solved by Fourier-transforming it into the frequency domain. Using the Fourier transform $f(t) = \frac{1}{2\pi}\int_{-\infty}^{+\infty} f(\omega)e^{i\omega t}d\omega$, we obtain the position and momentum fluctuations of the graphene sheet,

$$\delta y(\omega) = A_1(\omega)\xi_y(\omega) + B_1(\omega)\delta X_c^{in}(\omega) + C_1(\omega)\delta Y_c^{in}(\omega)$$
$$+ D_1(\omega)\delta X_a^{in}(\omega) + E_1(\omega)\delta Y_a^{in}(\omega),$$

$$\delta p_y(\omega) = A_2(\omega)\xi_y(\omega) + B_2(\omega)\delta X_c^{in}(\omega) + C_2(\omega)\delta Y_c^{in}(\omega)$$
$$+ D_2(\omega)\delta X_a^{in}(\omega) + E_2(\omega)\delta Y_a^{in}(\omega), \quad (8)$$

where

$$A_1(\omega) = \frac{\omega_m}{d(\omega)}\left[\beta_3(\kappa + i\omega)^2 + \Delta_{\text{eff}}\left(\beta_3\Delta_{\text{eff}} + \chi_3^2\Omega_c\right)\right],$$

$$B_1(\omega) = -\frac{\sqrt{2\gamma_a}}{d(\omega)}[(i\omega + \gamma_a)\beta_5\omega_m],$$

$$C_1(\omega) = -\frac{\sqrt{2\gamma_a}}{d(\omega)}[\beta_5\omega_m\Omega_c],$$

$$D_1(\omega) = -\frac{\sqrt{2\kappa}}{d(\omega)}[(\kappa + i\omega)\omega_m\beta_6],$$

$$E_1(\omega) = \frac{\sqrt{2\kappa}}{d(\omega)}(\Delta_{\text{eff}}\omega_m\beta_6),$$

$$A_2(\omega) = \frac{i\omega}{d(\omega)}\left[\beta_3(\kappa + i\omega)^2 + \Delta_{\text{eff}}\left(\beta_3\Delta_{\text{eff}} + \chi_3^2\Omega_c\right)\right],$$

$$B_2(\omega) = -\frac{\sqrt{2\gamma_a}}{d(\omega)}[i\omega(i\omega + \gamma_a)\beta_5],$$

$$C_2(\omega) = -\frac{\sqrt{2\gamma_a}}{d(\omega)}[i\omega\beta_5\Omega_c],$$

$$D_2(\omega) = -\frac{\sqrt{2\kappa}}{d(\omega)}[i\omega(\kappa + i\omega)\beta_6],$$

$$E_2(\omega) = \frac{\sqrt{2\kappa}}{d(\omega)}(i\omega\Delta_{\text{eff}}\beta_6).$$

$$(9)$$

In addition, in order to analyze the quantum coherence of the hybrid optomechanical system, we also need to derive the expressions of the quadratures of the cavity field:

$$\delta X_a(\omega) = A_3(\omega)\xi_y(\omega) + B_3(\omega)\delta X_c^{in}(\omega) + C_3(\omega)\delta Y_c^{in}(\omega)$$
$$+ D_3(\omega)\delta X_a^{in}(\omega) + E_3(\omega)\delta Y_a^{in}(\omega),$$

$$\delta Y_a(\omega) = A_4(\omega)\xi_y(\omega) + B_4(\omega)\delta X_c^{in}(\omega) + C_4(\omega)\delta Y_c^{in}(\omega)$$
$$+ D_4(\omega)\delta X_a^{in}(\omega) + E_4(\omega)\delta Y_a^{in}(\omega), \quad (10)$$

where

$$A_3(\omega) = \frac{1}{d(\omega)}(\Delta_{\text{eff}}\omega_m\beta_6),$$

$$B_3(\omega) = -\frac{\sqrt{2\gamma_a}}{d(\omega)}[(i\omega + \gamma_a)\Delta_{\text{eff}}\beta_7],$$

$$C_3(\omega) = -\frac{\sqrt{2\gamma_a}}{d(\omega)}(\Delta_{\text{eff}}\beta_7\Omega_c),$$

$$D_3(\omega) = \frac{\sqrt{2\kappa}}{d(\omega)}[(\kappa + i\omega)\beta_8],$$

$$E_3(\omega) = -\frac{\sqrt{2\kappa}}{d(\omega)}(\Delta_{\text{eff}}\beta_8),$$

$$A_4(\omega) = -\frac{1}{d(\omega)}[(\kappa + i\omega)\omega_m\beta_6],$$

$$B_4(\omega) = \frac{\sqrt{2\gamma_a}}{d(\omega)}[(\kappa + i\omega)(i\omega + \gamma_a)\beta_7],$$

$$C_4(\omega) = \frac{\sqrt{2\gamma_a}}{d(\omega)}[(\kappa + i\omega)\beta_7\Omega_c],$$

$$D_4(\omega) = \frac{\sqrt{2\kappa}}{d(\omega)}\left[(i\omega + \gamma_a)^2\left(\beta_1\Delta_{\text{eff}} + \chi_2^2\omega_m\right) + \Omega_c\left(\beta_2\Delta_{\text{eff}}\right.\right.$$
$$\left.\left. + \beta_1\chi_3^2 + 2\chi_1\chi_2\chi_3\omega_m + \chi_2^2\omega_m\Omega_c\right)\right],$$

$$E_4(\omega) = \frac{\sqrt{2\kappa}}{d(\omega)}[(\kappa + i\omega)\beta_8]. \quad (11)$$

In Eqs. (9) and (11), we define $d(\omega) = (\kappa + i\omega)^2\beta_8 + \Delta_{\text{eff}}D_4(\omega)$, $\beta_1(\omega) = -\omega^2 + i\omega\gamma_m + \omega_m\omega_{m0}$, $\beta_2(\omega) = -\chi_1^2\omega_m + \beta_1\Omega_c$, $\beta_3(\omega) = (i\omega + \gamma_a)^2 + \Omega_c^2$, $\beta_4(\omega) = (\kappa + i\omega)^2 + \Delta_{\text{eff}}^2$, $\beta_5(\omega) = \beta_4\chi_1 - \Delta_{\text{eff}}\chi_2\chi_3$, $\beta_6(\omega) = \beta_3\chi_1 + \Omega_c\chi_1\chi_3$, $\beta_7(\omega) = \beta_1\chi_3 + \chi_1\chi_2\omega_m$, and $\beta_8(\omega) = \beta_1(i\omega + \gamma_a)^2 + \beta_2\Omega_c$. In Eqs. (8) and (10), the first term in $\delta z(\omega)$ with $z = y, p_y, X_a, Y_a$ is from the thermal noise, the second and third terms are from the dissipation of the Bogoliubov mode, and the last two terms are from the radiation pressure of the cavity field. Further, using Eqs. (8) and (10), the spectra of fluctuations in the position and momentum of the graphene sheet and the quadrature of the cavity field are defined by

$$S_{zz}(\omega) = \int_{-\infty}^{\infty}\frac{d\Omega}{4\pi}\,e^{-i(\omega+\Omega)t}[\langle\delta z(\omega)\delta z(\Omega) + \delta z(\Omega)\delta z(\omega)\rangle]. \quad (12)$$

In order to obtain the power spectrum, we also calculate the nonzero correlation functions of all the noise sources in the frequency domain, which are defined by

$$\langle\xi(\omega)\xi(\Omega)\rangle = 2\pi\frac{\gamma_m}{\omega_m}\omega\left[\coth\left(\frac{\hbar\omega}{2k_BT}\right)+1\right]\delta(\omega+\Omega),$$

$$\langle\delta X_{a,c}^{in}(\omega)\delta X_{a,c}^{in}(\Omega)\rangle = \langle\delta Y_{a,c}^{in}(\omega)\delta Y_{a,c}^{in}(\Omega)\rangle = \pi\delta(\omega + \Omega). \quad (13)$$

Substituting Eqs. (8) and (10) into Eq. (12) and using the above correlation functions, the spectra of fluctuations in the position and momentum of the graphene sheet and the cavity

field quadratures can be obtained as

$$S_{zz}(\omega) = A_i(\omega)A_i(-\omega)\frac{\gamma_m}{\omega_m}\omega\beta_0$$
$$+ \frac{1}{2}[B_i(\omega)B_i(-\omega) + C_i(\omega)C_i(-\omega)]$$
$$+ \frac{1}{2}[D_i(\omega)D_i(-\omega) + E_i(\omega)E_i(-\omega)], \qquad (14)$$

with $i = 1,2,3,4$ and $\beta_0 = \coth(\frac{\hbar\omega}{2k_BT}) + 1$. Then, the mean-square fluctuation $\langle\delta z(t)^2\rangle$ in the position and momentum of the graphene sheet and the cavity field quadratures is

$$\langle\delta z(t)^2\rangle = \frac{1}{2\pi}\int_{-\infty}^{\infty} d\omega S_{zz}(\omega). \qquad (15)$$

Using the notation of the covariance matrix $\mathbf{V}(t)$, Eq. (15) corresponds to the diagonal element $V_{ii}(t) = \langle\delta z(t)^2\rangle$ in the covariance matrix $\mathbf{V}(t)$, i.e., $V_{11} = \langle\delta y(t)^2\rangle$, $V_{22} = \langle\delta p_y(t)^2\rangle$, $V_{33} = \langle\delta X_a(t)^2\rangle$, and $V_{44} = \langle\delta Y_a(t)^2\rangle$. The quantization of the quantum coherence for the graphene sheet and the cavity field requires calculation of nondiagonal matrix element $V_{ij}(t) = \langle\delta z(t)\delta z'(t) + \delta z'(t)\delta z(t)\rangle/2$ with $i,j = 1,2,3,4$ and $z,z' = y,p_y,X_a,Y_a$ in the second moments (covariance matrix) [33,61], i.e., $V_{12}(t) = \langle\delta y(t)\delta p_y(t) + \delta p_y(t)\delta y(t)\rangle/2$, $V_{34}(t) = \langle\delta X_a(t)\delta Y_a(t) + \delta Y_a(t)\delta X_a(t)\rangle/2$, and $V_{21} = V_{12}$, $V_{43} = V_{34}$. The nondiagonal matrix elements $V_{ij}(t)$ are determined by

$$V_{ij}(t) = \frac{1}{2\pi}\int_{-\infty}^{\infty} d\omega S_{zz'}(\omega), \qquad (16)$$

where

$$S_{zz'}(\omega) = \int_{-\infty}^{\infty}\frac{d\Omega}{4\pi} e^{-i(\omega+\Omega)t}[\langle\delta z(\omega)\delta z'(\Omega) + \delta z'(\Omega)\delta z(\omega)\rangle]. \qquad (17)$$

Similarly, the spectra of fluctuations for the nondiagonal elements can be derived analytically with Eqs. (8), (10), (13), and (17):

$$S_{zz'}(\omega) = \frac{1}{2}[A_i(\omega)A_j(-\omega) + A_j(\omega)A_i(-\omega)]\frac{\gamma_m}{\omega_m}\omega\beta_0$$
$$+ \frac{1}{4}[B_i(\omega)B_j(-\omega) + B_j(\omega)B_i(-\omega)]$$
$$+ \frac{1}{4}[C_i(\omega)C_j(-\omega) + C_j(\omega)C_i(-\omega)]$$
$$+ \frac{1}{4}[D_i(\omega)D_j(-\omega) + D_j(\omega)D_i(-\omega)]$$
$$+ \frac{1}{4}[E_i(\omega)E_j(-\omega) + E_j(\omega)E_i(-\omega)]. \qquad (18)$$

In terms of Eqs. (15) and (16), the covariance matrix of the graphene sheet, $\mathbf{V}_{\text{mec}}$, and the covariance matrix of the optical field, $\mathbf{V}_{\text{opt}}$, can be written, respectively, as

$$\mathbf{V}_{\text{mec}} = \begin{pmatrix} V_{11} & V_{12} \\ V_{21} & V_{22} \end{pmatrix}, \quad \mathbf{V}_{\text{opt}} = \begin{pmatrix} V_{33} & V_{34} \\ V_{43} & V_{44} \end{pmatrix}. \qquad (19)$$

IV. QUANTUM COHERENCE OF THE GRAPHENE SHEET AND THE CAVITY FIELD

In this section, we focus mainly on the characteristics of the coherence for the graphene sheet and the cavity field.

Using Eqs. (15), (16), and (19), the quantum coherence of the hybrid optomechanical system can be explored. For example, for a given bosonic mode $\hat{A}$ with the commutation relation $[\hat{A},\hat{A}^\dagger] = 1$, we can define the quadrature operators

$$\hat{X}_A = \frac{\hat{A} + \hat{A}^\dagger}{\sqrt{2}}, \quad \hat{Y}_A = \frac{\hat{A} - \hat{A}^\dagger}{\sqrt{2}i}. \qquad (20)$$

In particular, a Gaussian state ρ denoted by the collective operator $\hat{x} = (\hat{X}_A, \hat{Y}_A)$ can be fully described by its first moment $\vec{d} = (d_1,d_2) = \text{Tr}(\rho\hat{x})$ and second moment (the so-called covariance matrix) $\mathbf{V} = \begin{pmatrix} V_{XX} & V_{XY} \\ V_{YX} & V_{YY} \end{pmatrix}$. Furthermore, the coherence of any given one-mode Gaussian state $\rho(\mathbf{V},\vec{d})$ can be quantified in terms of the covariance matrix and the displacement vector [61]

$$C[\rho(\mathbf{V},\vec{d})] = -F(\nu) + F(2\bar{n} + 1), \qquad (21)$$

where $\nu = \sqrt{\text{Det}(\mathbf{V})}$, $\bar{n} = (V_{XX} + V_{YY} + d_1^2 + d_2^2 - 2)/4$, and $F(x) = \frac{x+1}{2}\log_2(\frac{x+1}{2}) - \frac{x-1}{2}\log_2(\frac{x-1}{2})$. It is notable that this measure is only valid for the Gaussian state under the operation of the (incoherent) Gaussian channel [33,61]. According to the covariance matrices in Eq. (19) and the definition in Eq. (21), the quantum coherence of the graphene sheet and the optical field can be expressed as

$$C_1 = C(\mathbf{V}_{\text{mec}}), \ C_2 = C(\mathbf{V}_{\text{opt}}). \qquad (22)$$

We now numerically evaluate the quantum coherence of the graphene sheet and the cavity field through Eq. (22). We select the accessible parameters of the cavity, i.e, the wavelength of the driving field, $\lambda_p \simeq 780$ nm, and the cavity decay rate $\kappa = 2\pi \times 2 \times 10^5$ Hz. In addition, we select the parameters of the atom, i.e., the mass of a single atom, $m_a = 1.42 \times 10^{-25}$ kg, the atomic number $N = 1 \times 10^4$, the weak atom-field coupling rate $U_{1s} = 2\pi$ Hz, the effective pump-atom detuning $\Delta_{as} = 2\pi \times 3 \times 10^8$ Hz, the free-space spontaneous emission rate $\Gamma_0 = 2\pi \times 6.1 \times 10^6$ Hz, the bare transition frequency $\omega_0 \simeq \omega_p$, and the dissipation rate of the Bogoliubov mode, $\gamma_a = 2\pi \times 1000$ Hz [62,63]. Additional parameters included the effective mass of the oscillating graphene, $M = 2.81 \times 10^{-18}$ kg, the oscillation frequency of the graphene sheet, $\omega_m = 2\pi \times 5 \times 10^6$ Hz, the damping rate $\gamma_M = 2\pi \times 30$ Hz, the temperature of the environment, $T = 10$ mK, the Fermi level $\mu = 0.8\hbar\omega_0$, and $\gamma_g = \omega_0$ [52]. We consider that the cavity is driven on its red sideband; i.e., $\Delta_{\text{eff}} = -\omega_m$.

The changes of the quantum coherence C_1 and C_2 as a function of the driving power P with different distance d (different vacuum coupling λ_0) are shown in Figs. 2 and 3. From Figs. 2 and 3, it is found that, in the absence of the external driving laser, the quantum coherence of the mechanical mode and the cavity mode always approaches zero with different distances. This is because the effective optomechanical coupling G_{ya} and the effective atom-graphene coupling G_{yc} are proportional to the steady-state photon number in the system. Therefore, when the external driving power is zero, both couplings G_{ya} and G_{yc} do not exist. Consequently, the quantum coherence of the system cannot be generated. With the increase of the driving power, the values of C_1 and C_2 increase monotonously, which means that the quantum coherence of the optomechanical system is gradually established. Comparing Fig. 2 with Fig. 3, we found that, with the same parameters, the degree of coherence of
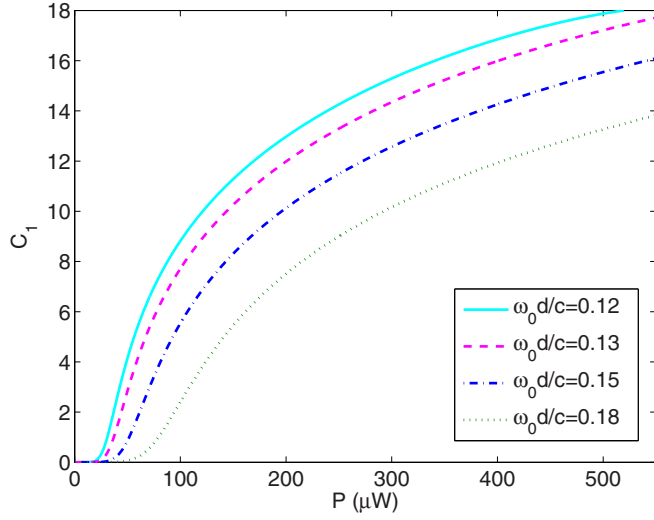
FIG. 2. The quantum coherence of the graphene sheet as a function of the input laser power P with different distances. The other parameter values are $\lambda_p \simeq 780$ nm, $\kappa = 2\pi \times 2 \times 10^5$ Hz, $m_a = 1.42 \times 10^{-25}$ kg, $N = 10^4$, $U_{1s} = 2\pi$ Hz, $\Delta_{as} = 2\pi \times 3 \times 10^8$ Hz, $\Gamma_0 = 2\pi \times 6.1 \times 10^6$ Hz, $\omega_0 \simeq \omega_p$, $\gamma_a = 2\pi \times 1000$ Hz, $M = 2.81 \times 10^{-18}$ kg, $\omega_m = 2\pi \times 5 \times 10^6$ Hz, $\gamma_m = 2\pi \times 30$ Hz, $T = 10$ mK, $\mu = 0.8\hbar\omega_0$, $\gamma_g = \omega_0$, and $\Delta_{\text{eff}} = -\omega_m$.

the cavity field is always larger than that of the graphene; i.e., $C_2 > C_1$. Physically, this feature of coherence results from the fact that the environmental incoherence of the optical field, i.e., the zero-point fluctuation, is much less than the incoherence of the thermal noise associated with the graphene sheet [33]. Further, for the same driving power, Fig. 2 shows that C_1 increases with the decrease of d and therefore the coherence of the mechanical motion in the optomechanical system is enhanced by the increase of the vacuum-induced coupling. In contrast, the degree of coherence in the cavity field, C_2, in Fig. 3 decreases significantly in the region of a large driving power with the decrease of d. The increase of C_1 with the decrease of d and the decrease of C_2 at the same time

means that the coherence in the system can be transferred from the optical into the mechanical mode, which results from the effective optomechanical interaction G_{ya} being of the form of the beam splitter in the red-detuned regime $\Delta_{\text{eff}} = -\omega_m$ with the resolved sideband condition $\omega_m > \kappa$ [33,64].

Apart from the vacuum-induced coupling, the effective optomechanical interaction G_{ya} is related to the optical lattice potential U_{1s}. In Figs. 4 and 5, we depicted the quantum coherences C_1 and C_2 as a function of the driving power P with different lattice potentials U_{1s}. From Figs. 4 and 5, we can see clearly that C_1 increases with the increase of U_{1s} while C_2 decreases at the same time in the region of large driving power. These results indicate that one could manipulate the quantum coherence of an optomechanical system by adjusting

FIG. 4. The quantum coherence of the graphene sheet as a function of the input laser power P with different optical lattice potentials. $\omega_0 d/c = 0.15$, and other parameter values are the same as in Fig. 2.
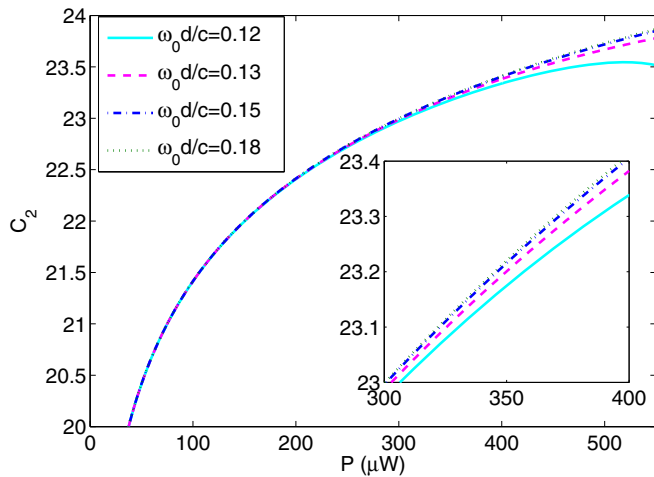

FIG. 3. The quantum coherence of the optical field as a function of the input laser power P with different distances. Other parameter values we select are the same as in Fig. 2.
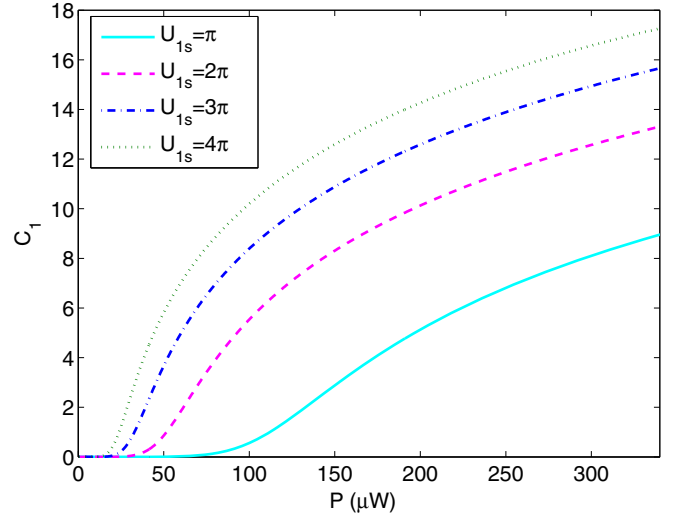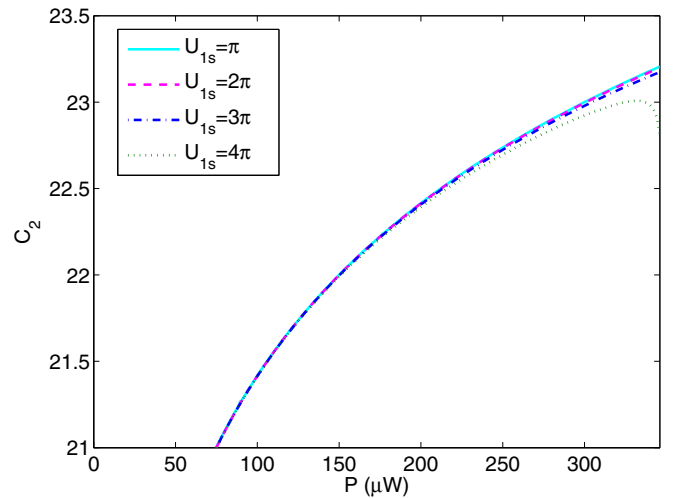

FIG. 5. The quantum coherence of the optical field as a function of the input laser power P with different optical lattice potentials. Other parameter values are the same as in Fig. 4.
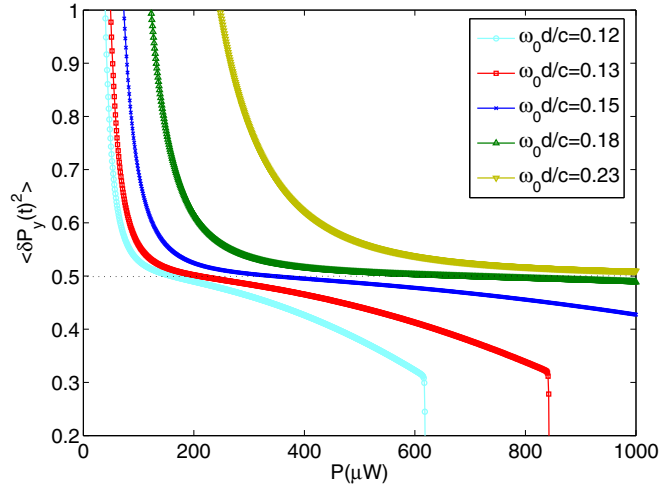
FIG. 6. The mean-square fluctuation $\langle \delta p_y(t)^2 \rangle$ as a function of the input laser power P with different distances. Other parameter values we select are the same as in Fig. 2.

FIG. 7. The mean-square fluctuation $\langle \delta p_y(t)^2 \rangle$ as a function of the input laser power P with different optical lattice potential. The other parameter values we select are the same as in Fig. 2.

the optical lattice potential U_{1s} or the atom-field coupling strength g_0 between the atoms and the cavity field.

V. MECHANICAL SQUEEZING OF THE GRAPHENE SHEET

In this section, we analyze the mechanical squeezing by numerically evaluating the mean-square fluctuation in the position and momentum of the graphene sheet. From Eq. (15), the mean-square fluctuations in the position and momentum of the graphene sheet, $V_{11} = \langle \delta y(t)^2 \rangle$ and $V_{22} = \langle \delta p_y(t)^2 \rangle$, satisfy the Heisenberg uncertainty principle,

$$\langle \delta y(t)^2 \rangle \langle \delta p_y(t)^2 \rangle \geqslant \left| \tfrac{1}{2} [y, p_y] \right|^2, \qquad (23)$$

where $[y, p_y] = i$. If either $\langle \delta y(t)^2 \rangle$ or $\langle \delta p_y(t)^2 \rangle$ is below 0.5, the state of the mechanical oscillator exhibits quadrature squeezing. The degree of the squeezing can be evaluated to be $-10 \log_{10} \frac{\langle \delta p_y(t)^2 \rangle}{\langle \delta p_y(t)^2 \rangle_{\text{vac}}}$ in decibels [65], where the momentum variance of the vacuum state is $\langle \delta p_y(t)^2 \rangle_{\text{vac}} = 0.5$.

Through evaluating in detail the mean-square fluctuations in the position and momentum of the graphene sheet given by Eq. (15), we found that $\langle \delta y(t)^2 \rangle$ cannot be less than 0.5, but $\langle \delta p_y(t)^2 \rangle$ can be less than 0.5. Therefore, we focus on the discussion of the mean-square fluctuation $\langle \delta p_y(t)^2 \rangle$. The variations of the mean-square fluctuation $\langle \delta p_y(t)^2 \rangle$ as a function of the driving power P with the different distances and different potentials U_{1s} are shown in Figs. 6 and 7. From Fig. 6, it is seen that $\langle \delta p_y(t)^2 \rangle$ decreases monotonously with the increase of the driving power. Further, when the distance between the atoms and the graphene sheet is large, i.e., $\omega_0 d/c = 0.23$, the mean-square fluctuation $\langle \delta p_y(t)^2 \rangle$ is always larger than 0.5 in the selected region of driving power; thus there is no squeezing in the momentum fluctuation of the graphene sheet. However, when the distance d becomes small, i.e., $\omega_0 d/c \lesssim 0.18$, the mean-square fluctuation $\langle \delta p_y(t)^2 \rangle$ can be less than 0.5. Hence the vacuum-induced coupling between the atoms and the graphene sheet in the hybrid optomechanical
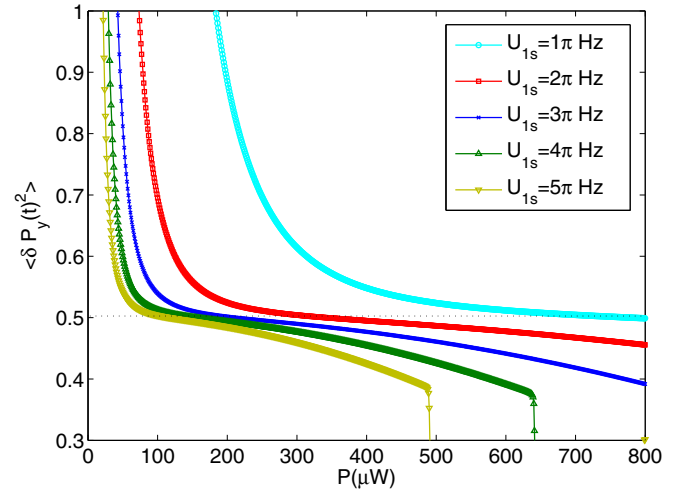
system helps realize the momentum squeezing of the graphene sheet. Furthermore, it is observed that the minimum values of $\langle \delta p_y(t)^2 \rangle$ for different d are the same, i.e., $\langle \delta p_y(t)^2 \rangle \simeq 0.3$, which holds uniformly at different driving power P. The corresponding maximum momentum squeezing is about 40% and the degree of the squeezing is about 2.22 dB. In Fig. 6, there is a sharp decline in the squeezing curve at a special driving power P, which decreases with the decrease of distance d. This is because in the region beyond the critical driving power, the condition that all the eigenvalues of the matrix J have negative real parts cannot be satisfied so the optomechanical system operates in the unstable regime. In Fig. 7, the driving power P corresponding to the minimum values of $\langle \delta p_y(t)^2 \rangle$ decreases with the increase of U_{1s}.

VI. THE SPECTRUM AND SQUEEZING OF THE OUTPUT FIELD

In this section, we analyze the spectrum of the output field and its squeezing. Using the quadrature fluctuation δX_a and δY_a of the cavity field in Eq. (10) and the input-output relation $a_{\text{out}} = \sqrt{2\kappa} a - a_{\text{in}}$ [66], we can get the fluctuation $\delta a_{\text{out}}(\omega)$ of the output field. Correspondingly, the quadrature fluctuation of the output field can be defined as

$$\delta Z_{\text{out}}(\omega) = \frac{1}{\sqrt{2}} [\delta a_{\text{out}}(\omega) e^{-i\phi} + \delta a_{\text{out}}(-\omega)^\dagger e^{i\phi}], \qquad (24)$$

where ϕ is the measurement phase angle depending on the local oscillator [65]. When $\phi = 0$, $\delta Z_{\text{out}}(\omega) = \delta X_{a\text{out}}(\omega)$, which denotes the amplitude fluctuation of the output field. When $\phi = \frac{\pi}{2}$, $\delta Z_{\text{out}}(\omega) = \delta Y_{a\text{out}}(\omega)$, which is the phase fluctuation of the output field. Further, the expression of the quadrature fluctuation $\delta Z_{\text{out}}(\omega)$ of the output field can be calculated as

$$\delta Z_{\text{out}}(\omega) = A_Z(\omega) \xi_y(\omega) + B_Z(\omega) \delta X_c^{in}(\omega) + C_Z(\omega) \delta Y_c^{in}(\omega)$$

$$+ D_Z(\omega) \delta X_a^{in}(\omega) + E_Z(\omega) \delta Y_a^{in}(\omega), \qquad (25)$$

where

$$A_Z(\omega) = \sqrt{2\kappa}[A_3(\omega)\cos\phi + A_4(\omega)\sin\phi],$$

$$B_Z(\omega) = \sqrt{2\kappa}[B_3(\omega)\cos\phi + B_4(\omega)\sin\phi],$$

$$C_Z(\omega) = \sqrt{2\kappa}[C_3(\omega)\cos\phi + C_4(\omega)\sin\phi],$$

$$D_Z(\omega) = \left[\sqrt{2\kappa}D_3(\omega) - \frac{1}{d(\omega)}\right]\cos\phi + \sqrt{2\kappa}D_4(\omega)\sin\phi,$$

$$E_Z(\omega) = \sqrt{2\kappa}E_3(\omega)\cos\phi + \left[\sqrt{2\kappa}E_4(\omega) - \frac{1}{d(\omega)}\right]\sin\phi. \tag{26}$$

It is noted that the output power spectrum of the phase quadrature with the optical field is an interesting quantity that is experimentally measurable by the homodyne measurement of the light [58]. Here, we define the spectrum of the quadrature fluctuation $\delta Z_{\text{out}}(\omega)$ of the output field as

$$S_{Z\text{out}}(\omega) = \int_{-\infty}^{\infty} \frac{d\Omega}{4\pi} e^{-i(\omega+\Omega)t} [\langle \delta Z_{\text{out}}(\omega)\delta Z_{\text{out}}(\Omega)\rangle + \langle \delta Z_{\text{out}}(\Omega)\delta Z_{\text{out}}(\omega)\rangle]. \tag{27}$$

Using the nonzero correlation functions of the thermal and vacuum noises in the frequency domain [Eq. (13)], the spectrum of the quadrature fluctuation $\delta Z_{\text{out}}(\omega)$ of the output field can be written as

$$S_{Z\text{out}}(\omega) = A_Z(\omega)A_Z(-\omega)\frac{\gamma_m}{\omega_m}\omega\beta_0$$

$$+ \frac{1}{2}[B_Z(\omega)B_Z(-\omega) + C_Z(\omega)C_Z(-\omega)]$$

$$+ \frac{1}{2}[D_Z(\omega)D_Z(-\omega) + E_Z(\omega)E_Z(-\omega)]. \tag{28}$$

When the value of the quadrature fluctuation is smaller than that of the vacuum state, i.e., $S_{Z\text{out}}(\omega) < 1/2$, the output field is also squeezed.

In Fig. 8, we show the plot of the spectrum $S_{Z\text{out}}(\omega)$ of the phase fluctuation of the output field as a function of the normalized frequency ω/ω_m when $\phi = \pi/2$ and $P = 1$ mW without the vacuum-induced coupling ($d \to \infty$) or with the vacuum-induced coupling ($\omega_0 d/c = 0.15$). In the absence of the vacuum-induced coupling, the spectrum of the output field, $S_{Z\text{out}}(\omega)$, has only one peak, at $\omega = \omega_m$. This situation is changed when the vacuum-induced coupling is included. In the presence of the vacuum-induced coupling, i.e., $\omega_0 d/c = 0.15$, the single peak is split so that the spectrum $S_{Z\text{out}}(\omega)$ displays two discrete peaks, which corresponds to the normal-mode splitting of the output field [67]. The normal-mode splitting in the optomechanical system results from the effective optomechanical coupling between the graphene sheet and the cavity field, mediated by the atomic ensemble. Further, we can see from Fig. 8 that the separation of the splitting peaks increases with the decrease of the distance d, which determines the strength of the vacuum-induced coupling λ_0. In addition, the squeezing in the phase fluctuation of the output field exists in the presence of the vacuum-induced coupling, i.e., $S_{Z\text{out}}(\omega) < 1/2$ at $\omega = \omega_m$. In contrast, the phase squeezing does not exist around $\omega/\omega_m = 1$ when the vacuum-induced coupling is removed. The measurement of the phase
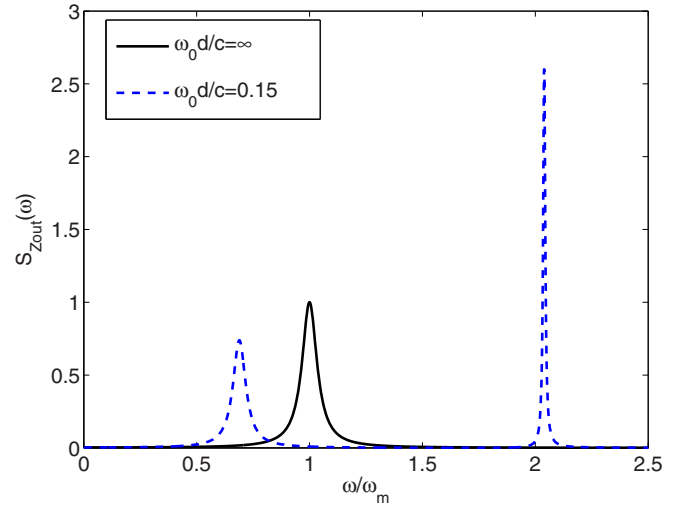

FIG. 8. The spectrum $S_{Z\text{out}}(\omega)$ of the phase fluctuation of the output field is plotted as a function of the normalized frequency ω/ω_m when $\phi = \pi/2$ and $P = 1$ mW in the absence and presence of the vacuum-induced coupling. Other parameter values are the same as in Fig. 2.

squeezing of the output field around $\omega/\omega_m = 1$ can be used to characterize the signature of the mechanical squeezing [65].

In the absence or presence of the vacuum-induced coupling, the contour plot of the spectrum $S_{Z\text{out}}(\omega)$ of the quadrature fluctuation of the output field versus the normalized frequency ω/ω_m and the phase ϕ/π is shown in Fig. 9. It is seen clearly that in the presence of the vacuum-induced coupling, the quadrature fluctuation $S_{Z\text{out}}(\omega)$ of the output field is always
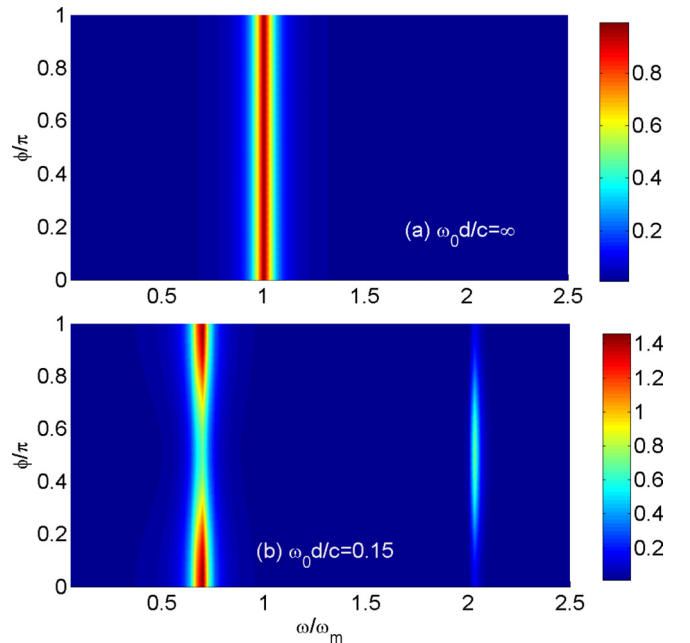

FIG. 9. The contour spectrum $S_{Z\text{out}}(\omega)$ of the quadrature fluctuation of the output field versus the normalized frequency ω/ω_m and the phase ϕ/π in the absence and presence of the vacuum-induced optomechanical coupling. Other parameter values are the same as in Fig. 8.

squeezed around $\omega/\omega_m = 1$ regardless of the value of the phase ϕ. These results and the measurement of the quadrature fluctuation of the output field may be used for demonstrating the vacuum-induced coupling between a graphene sheet and an atomic ensemble as well as detecting the mechanical squeezing of a graphene oscillator. We stress that in the present numerical examples we focus mainly on the regime of small atom-graphene distances, i.e., the order of the several tens of nanometers, so that the strong vacuum coupling between them is generated. Correspondingly, the macroscopic quantum coherence and the mechanical squeezing of the graphene oscillator can be more easily detected. However, it is noted that the experimental realizations may be a big challenge when the distance between the atomic ensemble and the graphene sheet is less than 100 nm. Even so, the generation of the macroscopic quantum properties in the hybrid optomechanical system with a relatively large atom-graphene distance is still possible by controlling the driving power of the system and the atom-field coupling strength.

VII. CONCLUSIONS

In conclusion, we analyzed a hybrid optomechanical system consisting of a suspended graphene sheet and an ultracold atomic ensemble trapped inside a Fabry-Pérot cavity. In the system the graphene sheet does not couple directly with the driven optical field. However, the ultracold atoms are close to a graphene sheet such that the vacuum-induced atom-graphene interaction is established, which mediates the effective optomechanical coupling between the mechanical oscillator and the cavity field. We showed that, in the presence of the mediated coupling, the macroscopic quantum coherence and mechanical squeezing of the graphene sheet in the optomechanical system can be attained with a moderate driving power. Further, the dependence on the distance between the atoms and the graphene sheet and on the atom-field coupling strength of the quantum coherence and mechanical squeezing are discussed in detail. We also calculate the spectrum and the squeezing of the output field and find that the phase fluctuation of the output field is squeezed when the vacuum-induced coupling between the atoms and the graphene sheet is included. The squeezing of the output field in the regime of the parameter $\omega \simeq \omega_m$ is useful for the study of the mechanical squeezing of the suspended graphene sheet. The splitting of the spectrum in the output field can also be used for estimating the vacuum coupling strength between an atom and a plane.

APPENDIX: VACUUM-INDUCED COUPLING λ_0

In order to calculate the vacuum-induced coupling λ_0, we should calculate the level shifts of the atom in its ground

and excited states [51,52,68,69]. In general, for an effective isotropic two-level system at position $\mathbf{r}$ near a plane, the shift of the transition rate is $\Delta\omega_a(\mathbf{r}) = \delta\omega_{ae}(\mathbf{r}) - \delta\omega_{ag}(\mathbf{r})$, where $\delta\omega_{ag}(\mathbf{r})$ and $\delta\omega_{ae}(\mathbf{r})$ are, respectively, the frequency shifts of the two-level system in its ground state and excited state. In terms of the classical dyadic Green's function $G(\mathbf{r},\mathbf{r},iu)$ evaluated at the imaginary frequency $\omega = iu$ [51,52], the two frequency shifts read

$$\delta\omega_{ag}(\mathbf{r}) = \frac{3c\Gamma_0}{\omega_0^2} \int_0^\infty du \frac{u^2}{\omega_0^2 + u^2} \text{Tr}\{G(\mathbf{r},\mathbf{r},iu)\} \quad \text{(A1)}$$

and

$$\delta\omega_{ae}(\mathbf{r}) = -\frac{\delta\omega_{ag}(\mathbf{r})}{3} - \frac{\pi c\Gamma_0}{\omega_0} \text{Tr Re}\{G(\mathbf{r},\mathbf{r},\omega_0)\}, \quad \text{(A2)}$$

respectively, where ω_0 and Γ_0 are the bare transition frequency and the decay rate of the two-level atom, respectively. For simplification, we approximate the Green's function of the graphene sheet by that of an infinite plane, assuming that the atom sits near the center of the graphene sheet. Moreover, the computation of the Green's function includes a reflection component from the plane located at interface $z = 0$, which describes the interaction of the two-level system with its own field reflected by this plane. In the vacuum regime of $z > 0$, the trace of this reflected component is $\text{Tr}\{G(z,z,\omega) = \frac{ic^2}{4\pi\omega^2} \int_0^\infty dk_\parallel \frac{k_\parallel}{K_0} e^{2izK_0}[(\frac{\omega}{c})^2 r_s + (k_\parallel^2 - K_0^2)r_p]$, where $K_0 = \sqrt{(\frac{\omega}{c})^2 - k_\parallel^2}$ and $k_\parallel$ is the parallel component of the wave vector; r_s and r_p are the Fresnel reflection coefficients for the s- and p-polarized waves. Considering the vacuum-graphene interface, the Fresnel reflection coefficients for the s- and p-polarized waves in the case of the vacuum-graphene interface are given by $r_s = -(1 + \frac{2K_0}{\mu_0\sigma\omega})^{-1}$ and $r_p = (1 + \frac{2\varepsilon_0\omega}{K_0\sigma})^{-1}$, which depend on the conductivity σ [70]. For a graphene sheet, the conductivity can be expressed as $\sigma(\omega) = \frac{e^2\mu}{\hbar\pi} \frac{i}{\omega + ir_g} + \frac{e^2}{4\hbar}[\Theta(\omega - 2\mu) + \frac{i}{\pi}\ln|\frac{\omega - 2\mu}{\omega + 2\mu}|]$, where μ is the Fermi energy and r_g is a phenomenological parameter describing the intraband losses [52,71,72]. Using the derived expression of the shift of the transition rate and the conductivity of the graphene sheet, the coupling strength λ_0 between a two-level atom and a graphene sheet can be calculated as [73]

$$\lambda_0(d) = \frac{-2c^3\Gamma_0}{\pi\omega_0^2} \int_0^\infty \frac{u^2}{\omega_0^2 + u^2} \int_0^\infty dk_\parallel k_\parallel e^{2idK_0}$$

$$\times \left[\left(\frac{\omega}{c}\right)^2 r_s + (k_\parallel^2 - K_0^2)r_p\right]$$

$$+ \text{Re}\frac{c^3\Gamma_0}{2\omega_0^3} \int_0^\infty dk_\parallel k_\parallel e^{2id\sqrt{(\frac{\omega_0}{c})^2 - k_\parallel^2}}$$

$$\times \left[\left(\frac{\omega_0}{c}\right)^2 r_s + \left(2k_\parallel^2 - \left(\frac{\omega_0}{c}\right)^2\right)r_p\right]. \quad \text{(A3)}$$

[1] S. E. Harris, J. E. Field, and A. Imamoglu, Phys. Rev. Lett. **64**, 1107 (1990).

[2] K. J. Boller, A. Imamoglu, and S. E. Harris, Phys. Rev. Lett. **66**, 2593 (1991).

[3] M. Fleischhauer, A. Imamoglu, and J. P. Marangos, Rev. Mod. Phys. **77**, 633 (2005).

[4] S. Y. Zhu and M. O. Scully, Phys. Rev. Lett. **76**, 388 (1996).

[5] M. D. Lukin, Rev. Mod. Phys. **75**, 457 (2003).

[6] M. M. Kash, V. A. Sautenkov, A. S. Zibrov, L. Hollberg, G. R. Welch, M. D. Lukin, Y. Rostovtsev, E. S. Fry, and M. O. Scully, Phys. Rev. Lett. **82**, 5229 (1999).

[7] F. Brennecke, S. Ritter, T. Donner, and T. Esslinger, Science **322**, 235 (2008).

[8] K. Zhang, W. Chen, M. Bhattacharya, and P. Meystre, Phys. Rev. A **81**, 013802 (2010).

[9] B. Chen, C. Jiang, and K. D. Zhu, Phys. Rev. A **83**, 055803 (2011).

[10] K. A. Yasir and W. M. Liu, Sci. Rep. **6**, 22651 (2016).

[11] D. Vitali, S. Gigan, A. Ferreira, H. R. Böhm, P. Tombesi, A. Guerreiro, V. Vedral, A. Zeilinger, and M. Aspelmeyer, Phys. Rev. Lett. **98**, 030405 (2007).

[12] F. Marquardt, J. G. E. Harris, and S. M. Girvin, Phys. Rev. Lett. **96**, 103901 (2006).

[13] O. Romero-Isart, A. C. Pflanzer, M. L. Juan, R. Quidant, N. Kiesel, M. Aspelmeyer, and J. I. Cirac, Phys. Rev. A **83**, 013803 (2011).

[14] D. E. Chang, C. A. Regal, S. B. Papp, D. J. Wilson, J. Ye, O. Painter, H. J. Kimble, and P. Zoller, Proc. Natl. Acad. Sci. U.S.A. **107**, 1005 (2010).

[15] T. Li, S. Kheifets, D. Medellin, and M. G. Raizen, Science **328**, 1673 (2010).

[16] Z. Q. Yin, T. Li, and M. Feng, Phys. Rev. A **83**, 013816 (2011).

[17] W. Nie, Y. Lan, Y. Li, and S. Zhu, Phys. Rev. A **86**, 063809 (2012).

[18] M. Bhattacharya and P. Meystre, Phys. Rev. Lett. **99**, 073601 (2007).

[19] Y. Li, L. A. Wu, and Z. D. Wang, Phys. Rev. A **83**, 043804 (2011).

[20] A. Schliesser, P. Del'Haye, N. Nooshi, K. J. Vahala, and T. J. Kippenberg, Phys. Rev. Lett. **97**, 243905 (2006).

[21] E. Verhagen, S. Deléglise, S. Weis, A. Schliesser, and T. J. Kippenberg, Nature (London) **482**, 63 (2012).

[22] J. D. Teufel *et al.*, Nature (London) **475**, 359 (2011).

[23] F. Xue, Y. X. Liu, C. P. Sun, and F. Nori, Phys. Rev. B **76**, 064305 (2007).

[24] Y. Li, Y. D. Wang, F. Xue, and C. Bruder, Phys. Rev. B **78**, 134301 (2008).

[25] C. Genes, A. Mari, P. Tombesi, and D. Vitali, Phys. Rev. A **78**, 032316 (2008).

[26] M. C. Kuzyk, S. J. van Enk, and H. Wang, Phys. Rev. A **88**, 062341 (2013).

[27] Y. D. Wang and A. A. Clerk, Phys. Rev. Lett. **110**, 253601 (2013).

[28] X. Yang, Y. Ling, X. Shao, and M. Xiao, Phys. Rev. A **95**, 052303 (2017).

[29] I. Wilson-Rae, N. Nooshi, W. Zwerger, and T. J. Kippenberg, Phys. Rev. Lett. **99**, 093901 (2007).

[30] F. Marquardt, J. P. Chen, A. A. Clerk, and S. M. Girvin, Phys. Rev. Lett. **99**, 093902 (2007).

[31] X. W. Xu, Y. J. Zhao, and Y. X. Liu, Phys. Rev. A **88**, 022325 (2013).

[32] M. Abdi and M. J. Hartmann, New J. Phys. **17**, 013056 (2015).

[33] Q. Zheng, J. Xu, Y. Yao, and Y. Li, Phys. Rev. A **94**, 052314 (2016).

[34] M. Aspelmeyer, T. J. Kippenberg, and F. Marquardt, Rev. Mod. Phys. **86**, 1391 (2014).

[35] A. A. Clerk, F. Marquardt, and K. Jacobs, New J. Phys. **10**, 095010 (2008).

[36] R. A. Norte, J. P. Moura, and S. Gröblacher, Phys. Rev. Lett. **116**, 147202 (2016).

[37] S. M. Meenehan, J. D. Cohen, S. Gröblacher, J. T. Hill, A. H. Safavi-Naeini, M. Aspelmeyer, and O. Painter, Phys. Rev. A **90**, 011803 (2014).

[38] Y. Tsaturyan, A. Barg, E. S. Polzik, and A. Schliesser, Nat. Nanotechnol. **12**, 776 (2017).

[39] A. Mari and J. Eisert, Phys. Rev. Lett. **103**, 213603 (2009).

[40] W. J. Gu and G. X. Li, Opt. Express **21**, 020423 (2013).

[41] S. Huang and G. S. Agarwal, Phys. Rev. A **82**, 033811 (2010).

[42] X. Y. Lü, J. Q. Liao, L. Tian, and F. Nori, Phys. Rev. A **91**, 013834 (2015).

[43] M. Benito, C. Sánchez Muñoz, and C. Navarrete-Benlloch, Phys. Rev. A **93**, 023846 (2016).

[44] C. M. Caves, K. S. Thorne, R. W. P. Drever, V. D. Sandberg, and M. Zimmermann, Rev. Mod. Phys. **52**, 341 (1980).

[45] N. Didier, J. Bourassa, and A. Blais, Phys. Rev. Lett. **115**, 203601 (2015).

[46] S. Lloyd and S. L. Braunstein, Phys. Rev. Lett. **82**, 1784 (1999).

[47] S. Camerer, M. Korppi, A. Jöckel, D. Hunger, T. W. Hänsch, and P. Treutlein, Phys. Rev. Lett. **107**, 223001 (2011).

[48] A. V. Parafilo, S. I. Kulinich, L. Y. Gorelik, M. N. Kiselev, R. I. Shekhter, and M. Jonson, Phys. Rev. Lett. **117**, 057202 (2016).

[49] S. Haroche and J. M. Raimond, *Exploring the Quantum: Atoms, Cavities and Photons* (Oxford University Press, New York, 2006).

[50] O. Morsch and M. Oberthaler, Rev. Mod. Phys. **78**, 179 (2006).

[51] D. E. Chang, K. Sinha, J. M. Taylor, and H. J. Kimble, Nat. Commun. **5**, 4343 (2014).

[52] C. A. Muschik, S. Moulieras, A. Bachtold, F. H. L. Koppens, M. Lewenstein, and D. E. Chang, Phys. Rev. Lett. **112**, 223601 (2014).

[53] X. Z. Yuan, Phys. Rev. A **88**, 052317 (2013).

[54] C. Maschler and H. Ritsch, Phys. Rev. Lett. **95**, 260401 (2005).

[55] C. Maschler and H. Ritsch, Opt. Commun. **243**, 145 (2004).

[56] D. Nagy, P. Domokos, A. Vukics, and H. Ritsch, Eur. Phys. J. D **55**, 659 (2009).

[57] A. Dalafi and M. H. Naderi, J. Phys. B: At. Mol. Opt. Phys. **49**, 145501 (2016).

[58] V. Giovannetti and D. Vitali, Phys. Rev. A **63**, 023812 (2001).

[59] C. Gardiner and P. Zoller, *Quantum Noise: A Handbook of Markovian and Non-Markovian Quantum Stochastic Methods with Applications to Quantum Optics* (Springer, New York, 2004).

[60] E. X. De Jesus and C. Kaufman, Phys. Rev. A **35**, 5288 (1987).

[61] J. Xu, Phys. Rev. A **93**, 032111 (2016).

[62] W. Chen, D. S. Goldbaum, M. Bhattacharya, and P. Meystre, Phys. Rev. A **81**, 053833 (2010).

[63] M. Paternostro, G. De Chiara, and G. M. Palma, Phys. Rev. Lett. **104**, 243602 (2010).

[64] W. Nie, A. Chen, and Y. Lan, Phys. Rev. A **93**, 023841 (2016).

[65] G. S. Agarwal and S. Huang, Phys. Rev. A **93**, 043844 (2016).

[66] D. F. Walls and G. J. Milburn, *Quantum Optics* (Springer-Verlag, Berlin, 1994).

[67] S. Huang and G. S. Agarwal, Phys. Rev. A **80**, 033807 (2009).

[68] S. Y. Buhmann, L. Knöll, D. G. Welsch, and H. T. Dung, Phys. Rev. A **70**, 052117 (2004).

[69] S. Y. Buhmann and D. G. Welsch, Prog. Quantum Electron. **31**, 51 (2007).

[70] L. A. Falkovsky, J. Phys.: Conf. Ser. **129**, 012004 (2008).

[71] B. Wunsch, T. Stauber, F. Sols, and F. Guinea, New J. Phys. **8**, 318 (2006).

[72] T. Stauber, N. M. R. Peres, and A. K. Geim, Phys. Rev. B **78**, 085432 (2008).

[73] W. J. Nie, A. X. Chen, and Y. H. Lan, Opt. Express **23**, 030970 (2015).